Design Optimization Procedure of Air-Cored Resonant Induction Machines

Zhao Jin
Department of Electrical and Electronic Engineering
The University of Manchester
Manchester, U.K.
zhao.jin@manchester.ac.uk

Matteo F. Iacchetti
Department of Electrical and Electronic Engineering
The University of Manchester
Manchester, U.K.
matteo.iacchetti@manchester.ac.uk

Alexander C. Smith
Department of Electrical and Electronic Engineering
The University of Manchester
Manchester, U.K.
sandy.smith@manchester.ac.uk

Rajesh P. Deodhar
IMRA Europe S.A.S.
UK Research Centre
Brighton, U.K.
rd@imra-ukrc.com

Yoshiyuki Komi
Aisin Seiki Co., Ltd.
Kariya, Japan
yk@imra-ukrc.com

Ahmad Anad Abduallah
IMRA Europe S.A.S.
UK Research Centre
Brighton, U.K.
aa@imra-ukrc.com

Chiaki Umemura
Aisin Seiki Co., Ltd.
Kariya, Japan
cu@imra-ukrc.com

***Abstract*—The air-cored resonant induction machine removes the iron core which makes its magnetic field truly 3-D in nature. The axial conductors and end windings now both become active components contributing to torque production. The whole winding therefore needs to be considered in the design process. Conventional 3-D finite element analysis has large computational costs and is hard to integrate into the design optimization. This paper presents a new design optimization procedure for air-cored resonant induction machines using closed-form solutions of Neumann integrals which are computationally fast and considers the 3-D magnetic field distributions created by the air-cored coils. Optimized designs for two tuning options in the literature: option I with stator capacitors only and option II with both stator and rotor capacitors, are presented. The optimization trends with respect to different machine parameters are also discussed.**

Keywords—Air core, resonance, 3-D inductance, closed-form expressions, design trends.

NOMENCLATURE

a_s, a_r	Radial depth of the stator, rotor winding.
b_s, b_r	Stator, rotor coil pitch.
C_s, C_r	Stator, rotor capacitance.
c_i	Circumferential width on the baseline circle of the coil i cross-section.
g	Airgap length.
h_{cond}, h_{encap}	Density of the conductors, encapsulation.
J_s, J_r	Stator, rotor current density.
J_0	Current density constraint.
k_{asp}	Aspect ratio.
$k_{ew,s}$, $k_{ew,r}$	Stator, rotor end-winding length factor.
k_f	Fill factor.
L_s, L_r, M	Stator self-, rotor self-, magnetizing inductance in the equivalent circuit.
L_{si}	Self-inductance of coil i.
M_{ij}	Mutual inductance of coil i and coil j.
N_s, N_r	Stator, rotor number of turns in series per phase.
N_{slot}	Number of slots.
n_s	Synchronous speed.
P_m, P_{m0}	Mechanical power, required output power.
p_p	Number of pole pairs.
R_s, R_r, R_r'	Stator, rotor, referred rotor resistance.
r_{bs}, r_{br}	Stator, rotor mean excitation radius.
s, s_0, s_η	Slip, prescribed slip, peak-efficiency slip.
w, w_i	Axial length of the machine, axial length of the equivalent rectangular coil i.
X_{ls}, X_m, X_{lr}'	Stator leakage, magnetizing, referred rotor leakage reactance.
X_{Cs}, X_{Cr}'	Stator, referred rotor capacitor reactance.
η, η_{pk}	Efficiency, peak efficiency.

Subscripts and superscripts

ew, *wdg*	Related to end-winding, winding.
(I), (II)	Related to tuning option I, tuning option II.
i, j	Related to coil i, coil j.
s, r	Related to stator, rotor.

I. INTRODUCTION

The design features of removing magnetic cores and the advantages of reducing mass and eliminating iron losses draw growing interest recently in air-cored resonant induction machines (ACRIMs) for light-weight, low-inertia, and high-power-density applications. [1] and [2] present the electromagnetic model for both linear and radial-flux rotating ACRIMs. The analyses in [1] and [2] are based on a two-phase winding configuration, the expressions for self and mutual inductances, force and torque are derived and validated using finite element analysis (FEA). However, both analytic modeling and finite element (FE) validation are 2-D and do not consider the 3-D effects of air-cored coils. Also, the stationary and moving coils are assumed to have the same inductance and capacitance values, and the papers do not provide any insight into the design process. In addition, the rotor speed is assumed to be very small compared to the very high supply frequency of hundreds of kilohertz to several megahertz so the slip value is treated as close to unity in the analytic modeling. However, high-slip operation can lead to a very low efficiency for induction machines (IMs). [3] presents the equivalent circuit of ACRIMs with validation using FEA. The operating characteristics, including torque, efficiency, power factor, of radial-flux and axial-flux ACRIMs and

ACRIMs with cage rotors are investigated in [4] and [5]. However, these studies are again based on 2-D FEA and little information is provided regarding the ACRIM design process. [6] reports an experimental validation of an axial-flux ACRIM but only with a locked rotor. [7] proposes an ACRIM topology utilizing the frequency splitting phenomenon: the supply frequency is adjusted in accordance with the rotor position to produce attractive and repulsive forces between the stator and rotor. 2-D FE validations are included in the paper but only for a stationary rotor fixed at different angles and no experimental confirmation is provided for the operating principle. [8]-[9] compare four different capacitor tuning criteria and propose an ACRIM configuration using stator capacitors only, [10] presents the experimental validation of the tuning option on a spinning ACRIM prototype. However, [8]-[10] do not cover the design procedure. Considering there is no magnetic core in air-cored machines and therefore the magnetic field is inherently 3-D, [11] proposes a fast 3-D inductance estimation method for ACRIMs using closed-form expressions without relying on the computationally-demanding 3-D FEA, but the design optimization of ACRIMs is not discussed.

In this paper, a new design optimization procedure based on the 3-D inductance calculation method using closed-form solutions of Neumann integrals is presented, which is computationally fast, 3-D FEA free and considers 3-D effects of air-cored windings. Detailed design procedure, including the selection of operating point, tuning of the capacitors, optimization objective and constraints, are presented. Finally, optimized designs based on a particular specification are carried out and the results are compared with the variation of different ACRIM parameters to discuss the optimization trends.

II. Modeling of ACRIMs

A. Equivalent Circuit

The steady-state per-phase equivalent circuit of ACRIMs with both stator and rotor capacitors has been derived and validated in [10] and is shown in Fig. 1, where the stator and referred rotor resistances are R_s and R_r' respectively, the stator leakage, magnetizing and referred rotor leakage reactances are X_{ls}, X_m and X_{lr}' respectively, the stator capacitor and referred rotor capacitor reactances are X_{Cs} and X_{Cr}' respectively.

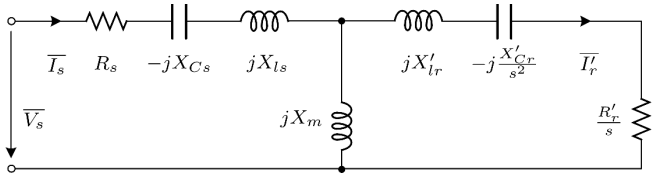

Fig. 1. Steady-state per-phase equivalent circuit of an ACRIM (motor convention).

B. Capacitor Tuning Options

The capacitor tuning criteria have been analyzed and compared in [9]. Two capacitor tuning options showing the potential of achieving better performances are selected and focused on in this article.

The first tuning option, denoted as *tuning I*, is to use stator capacitors only to cancel out the equivalent machine reactance seen from the stator terminals at a prescribed slip s_0. The required stator capacitor reactance is

$$X_{Cs}^{(\mathrm{I})} = \big(R_r'^2(X_{ls}+X_m)+s_0^2(X_{lr}'+X_m)(X_{ls}X_m + X_{lr}'(X_{ls}+X_m))\big)(R_r'^2+s_0^2(X_{lr}'+X_m)^2)^{-1} \quad (1)$$

This option removes the rotor capacitors so the rotor capacitor reactance $X_{Cr}'^{(\mathrm{I})} = 0$.

The second tuning option, *tuning II*, is to use both stator and rotor capacitors to compensate for the stator and rotor self-inductive reactances respectively, so the required stator and rotor capacitor reactances are

$$X_{Cs}^{(\mathrm{II})} = X_{ls}+X_m,\ X_{Cr}'^{(\mathrm{II})} = s_0^2(X_{lr}'+X_m) \quad (2)$$

It can be seen that, the rotor capacitance of tuning II and the stator capacitance of tuning I are both related to the prescribed slip value s_0, which means for fixed capacitors under a certain supply frequency, these tuning criteria can only be fulfilled at a single slip. In order to achieve a high-efficiency operation, the prescribed slip, which is the resonant point, is selected as the rated operating point and is set to the slip where the ACRIM achieves its peak efficiency, i.e., the peak-efficiency slip, s_η.

C. Peak-Efficiency Points

Based on the equivalent circuit, the general efficiency expression for ACRIM in motoring-mode can be derived as

$$\eta = \frac{(1-s)s^3R_r'X_m^2}{s^2R_r'(R_r'R_s+sX_m^2)+R_s(X_{Cr}'-s^2(X_{lr}'+X_m))^2} \quad (3)$$

substituting (1) and (2) into (3) respectively and analyzing the first derivative of efficiency with respect to slip, $\partial\eta/\partial s$, yields the peak-efficiency points for the two tuning options [9].

For tuning option I, the motoring-mode peak-efficiency slip $s_\eta^{(\mathrm{I})}$ and peak efficiency $\eta_{pk}^{(\mathrm{I})}$ are

$$s_\eta^{(\mathrm{I})} = \big(1+(1+X_m^2/(R_r'R_s)+(X_{lr}'+X_m)^2/R_r'^2)^{1/2}\big)^{-1} \quad (4)$$

$$\eta_{pk}^{(\mathrm{I})} = X_m^2\big(2R_r'R_s+X_m^2+2\big(R_s(R_r'^2R_s+R_r'X_m^2 + R_s(X_{lr}'+X_m)^2)\big)^{1/2}\big)^{-1} \quad (5)$$

This is also the peak-efficiency point for the pure air-cored IM without capacitors since (3) is independent of stator capacitance.

For tuning option II, the motoring-mode peak-efficiency point ($s_\eta^{(\mathrm{II})}$, $\eta_{pk}^{(\mathrm{II})}$) is

$$s_\eta^{(\mathrm{II})} = \big(1+(1+X_m^2/(R_r'R_s))^{1/2}\big)^{-1} \quad (6)$$

$$\eta_{pk}^{(\mathrm{II})} = X_m^2\big(2R_r'R_s+X_m^2+2(R_r'R_s(R_r'R_s+X_m^2))^{1/2}\big)^{-1} \quad (7)$$

Comparing (4) and (6), (5) and (7), it can be observed that, for a fixed air-cored IM design operated under the same supply frequency, option II is able to achieve higher peak efficiency than option I, and option II has a smaller peak-efficiency slip. Adding the rotor capacitor helps improve the peak efficiency achievable by ACRIMs because of the reduced rotor branch impedance at resonance.

Equations (4)-(7) are used for finding the maximum efficiency point in the design optimization routine. However, applying (4)-(7) requires the machine parameters to be estimated first.

D. Parameter Estimation

The machine parameters, i.e., the resistances and inductances in the equivalent circuit, can be determined as functions of the machine dimensions. Fig. 2 shows the idealized cross-section of an air-cored IM. The stator and rotor mean excitation radii, i.e., the radii of the stator and rotor baseline circles which locate at their centers, are denoted as r_{bs} and r_{br} respectively, the radial depth of the stator and rotor winding excitations are denoted as a_s and a_r respectively, the airgap length is denoted as g.

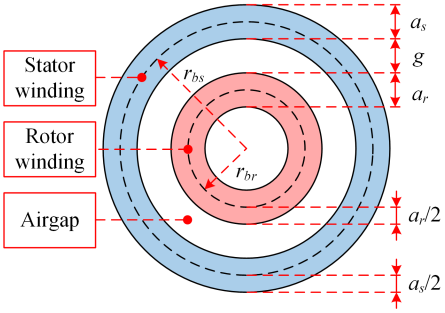

Fig. 2. Idealized cross-section of the air-cored IM.

All machine coils are assumed to be composed by straight axial parts of axial length w, and with the end windings extending outside which has the length equal to a semi-circle. The axial length w is related to the mean airgap diameter (r_{bs}+r_{br}) using a pre-set aspect ratio which is defined as

$$k_{asp} = (r_{bs} + r_{br})/w \tag{8}$$

The diameter of the semi-circular end is assumed to be equal to the coil pitch. For fully-pitched coils, the stator and rotor end-winding diameters are

$$b_s = 2r_{bs}\sin(\pi/(2p_p)),\ b_r = 2r_{br}\sin(\pi/(2p_p)) \tag{9}$$

where b_s and b_r are the stator and rotor coil pitches respectively, p_p is the number of pole pairs. The one-side end-winding lengths for stator and rotor coils are $l_{ew,s} = \pi r_{bs}\sin(\pi/(2p_p))$ and $l_{ew,r} = \pi r_{br}\sin(\pi/(2p_p))$ respectively. The end-winding length factor is the one-side end-winding length divided by the machine axial length,

$$\begin{aligned} k_{ew,s} &= \pi r_{bs}\sin(\pi/(2p_p))/w \\ k_{ew,r} &= \pi r_{br}\sin(\pi/(2p_p))/w \end{aligned} \tag{10}$$

where $k_{ew,s}$ and $k_{ew,r}$ are the end-winding length factors for stator and rotor respectively. The stator and rotor per-phase resistances can be subsequently calculated as

$$\begin{aligned} R_s &= 2\rho m w(1+k_{ew,s})N_s^2/(\pi r_{bs}a_s k_f) \\ R_r &= 2\rho m w(1+k_{ew,r})N_r^2/(\pi r_{br}a_r k_f) \end{aligned} \tag{11}$$

where ρ is the resistivity of the conductor material, m is the number of phases, k_f is the winding fill factor, N_s and N_r are the number of turns in series per phase for stator and rotor respectively.

Since the magnetic field in air-cored IMs is 3-D in nature, the inductance calculation needs to consider the entire winding including the effect of the end-windings. 3-D FEA can be computationally-heavy, and modeling the detailed end-winding shape to avoid conductors intersecting from design to design can also be time-consuming, so 3-D FEA can be hard to incorporate into an optimisation procedure. [11] proposes an analytic method for 3-D inductance calculation for air-cored windings which is computationally-fast and 3-D-FEA-free. It uses closed-form solutions of Neumann integrals for a pair of conductors with any mutual orientation, it is robust and can handle crossing points in the coil ends without being affected by numeric singularities and is suitable for analytic implementation without detailed modeling of end-winding shape and end-region arrangement in 3-D FEA.

Fig. 3 shows two arbitrary coils, coil i and coil j, in ACRIMs, where a_i and a_j are the radial depth and c_i and c_j are the circumferential width on the baseline circles of the cross-sections of coils i and j respectively, r_{bi} and r_{bj} are the baseline circle radii on which coils are located, γ_{ij} is the angle between the two coil axes, b_i and b_j are the coil pitches. It is assumed that the rectangular coil shape will provide a reasonable 3D model of real coils so the machine coil is firstly converted to an equivalent rectangle so that its end-winding coil shape has the same effective length as the semi-circular shape, as shown by the thick dashed lines in Fig. 3, where w_i and w_j are the axial depths for the equivalent rectangular coils and can be calculated as follows,

$$w_i = w + (\pi - 2)r_{bi}\sin(\pi/(2p_p)) \tag{12}$$

The coil resistance value does not change during this transform.

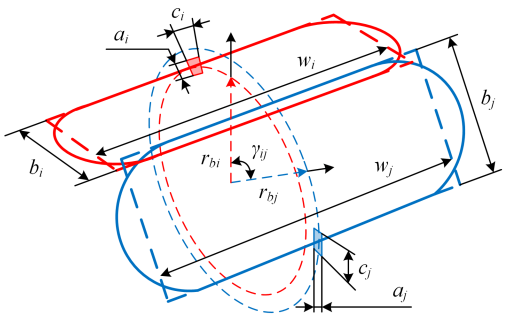

Fig. 3. Two arbitrary coils in the ACRIM.

Based on the winding inductance estimation method proposed in [11], the coils are represented by filaments located at their centers, which in practice are defined by two matrices containing vertex coordinates of central filaments of the two coils, $\mathbf{G_i}$ and $\mathbf{G_j}$. It is assumed that the coils have round cross-sections which have the same area as their original cross-sections. The self-inductance of coil i, L_{si}, is collected from the self-inductance of every conductor and the mutual inductance between each pair of conductors.

$$L_{si} = L(c_i, a_i, w_i, b_i) = L(c_i, a_i, \mathbf{G_i}) \tag{13}$$

The mutual inductance of coils i and j, M_{ij}, is the summation of the mutual inductances between all pairs of the straight segments from the two coils.

$$M_{ij} = M(w_i, b_i, r_{bi}, w_j, b_j, r_{bj}, \gamma_{ij}) = M(\mathbf{G_i}, \mathbf{G_j}) \tag{14}$$

The calculations of both self-inductance of a conductor and the mutual inductance of a pair of segments in (13) and (14) use closed-from solutions of Neumann integrals. However, the detailed expressions are very convoluted especially when the two segments are placed at different orientations, so only their structures are shown above [12].

The phase winding self and mutual inductances are then calculated by collecting the contributions from all coil self-inductances and coil-to-coil mutual inductances. It is worth mentioning that, by invoking the periodicity and symmetry features in the IM winding layout, redundant calculations can be avoided and the computation time can be further reduced. Finally, the equivalent circuit inductances, i.e., stator self-, rotor self- and magnetizing inductances, are merged from the winding inductances. The collection routine has been presented and validated in [11] and will not be repeated here.

III. Optimization Procedure of an ACRIM

A. Design Specification

This article focuses on the three-phase ACRIM electromagnetic design optimisation procedure. A benchmark design specification requires the air-cored resonant induction motor to output 10 kW shaft power with a 60 Vrms voltage supply. A current density constraint of 40 A/mm^2 is set for both stator and rotor so that no excessive cooling technologies are needed for short duty-cycle operation at this current density. Preliminary studies reveal that ACRIMs are able to achieve higher efficiency at higher speeds, considering the mechanical design challenge, the synchronous speed of 40k rpm and an airgap length of 2 mm are selected. Because tuning option II needs to connect rotor capacitors, a wound rotor is adopted. For manufacturing reasons, a fill factor of 0.6, a slot number of 36 are chosen, and a single-layer, fully-pitched, lap winding layout is used for both stator and rotor. The design specifications are summarized in TABLE I below.

TABLE I. Design Specifications

Specifications	Symbols	Parameters
Supply voltage	V_s	60 Vrms
Mechanical output power	P_{m0}	10 kW
Current density	J_0	40 A/mm^2
Synchronous speed	n_s	40k rpm
Airgap length	g	2 mm
Fill factor	k_f	0.6
Number of slots	N_{slot}	36

B. Optimization Procedure

Five key variables are selected to be optimized in the design procedure, these are the stator and rotor mean excitation radii, r_{bs} and r_{br}, the radial depth of the stator and rotor winding excitation, a_s and a_r and the stator number of turns per phase N_s. The stator and rotor are set arbitrarily to have the same number of turns so the stator-to-rotor turns ratio is 1. The five variables (r_{bs}, r_{br}, a_s, a_r, N_s) are bounded with minimum and maximum values as shown in TABLE II.

TABLE II. Lower and Upper Bounds for Optimization Variables

Variables	Unit	Lower bound	Upper bound
r_{bs}	mm	10	52.5
r_{br}	mm	5	50.5
a_s	mm	1	25
a_r	mm	1	25
N_s	(Turns)	10	200

Apart from the five optimization variables mentioned above, other IM parameters, such as the number of poles, synchronous frequency, airgap length, aspect ratio, number of slots, fill factor, turns ratio, etc., are left as pre-set values.

The ACRIM is designed to have its rated operating point and the resonant prescribed slip both at its peak-efficiency point. The optimization program starts from an initial set of (r_{bs}, r_{br}, a_s, a_r, N_s) within their lower and upper bounds, then calculates the equivalent circuit parameters based on the design variables and pre-set values. Consequently, the motoring-mode peak-efficiency points (s_η, η_{pk}) for tuning options I and II can be computed using (4)-(7). The prescribed slip s_0 is then known and the capacitances are tuned to resonate at the peak-efficiency slip, i.e., $s_0 = s_\eta$. Considering the supply voltage, the machine performance parameters including stator and rotor currents, torque, output power and other performance parameters can all be solved. The objective of the optimization is to search for the optimal combination of (r_{bs}, r_{br}, a_s, a_r, N_s) which maximizes the peak efficiency η_{pk}. whilst satisfying several constraints.

The linear constraints are as follows. The rotor winding half-depth should be smaller than the rotor winding mean radius because of the space taken up by the shaft and rotor inner supporting materials,

$$a_r/2 - r_{br} < 0 \tag{15}$$

Also, the stator and rotor baseline circle radii, the stator and rotor winding depths and the airgap length should follow the equality constraint shown in Fig. 2.

$$r_{bs} - a_s/2 - r_{br} - a_r/2 = g \tag{16}$$

Both constraints above are simple linear relations applied to design variables directly.

However, there are also nonlinear constraints involving computation results based on more complex nonlinear calculations such as the inductance estimation.

The first nonlinear constraint is that the motoring-mode peak-efficiency slip should fall in the slip range of 0 to 1,

$$0 < s_\eta < 1 \tag{17}$$

Secondly, the stator and rotor current density should stay within the specified limit. The stator and rotor winding current density, J_s and J_r, can be calculated as,

$$J_s = 2mI_s/(\pi r_{bs} a_s k_f),\ J_r = 2mI_r/(\pi r_{br} a_r k_f) \tag{18}$$

where I_s and I_r are the stator and rotor winding per-phase current rms values respectively. The current density constraints can then be expressed as,

$$J_s < J_0,\ J_r < J_0 \tag{19}$$

where J_0 is 40 A/mm^2. The two nonlinear constraints mentioned above are inequality constraints. In addition, the required output of 10kW yields an equality constraint,

$$P_m = P_{m0} = 10 \text{ kW} \tag{20}$$

where P_m is the mechanical power multiplied by the output torque and rotor speed at the peak-efficiency slip.

The optimization is carried out using the MATLAB Optimization Toolbox, multiple starting points and iterations are used to eliminate local minima and find the final optimized

design. The complete optimization procedure is summarized in Fig. 4.

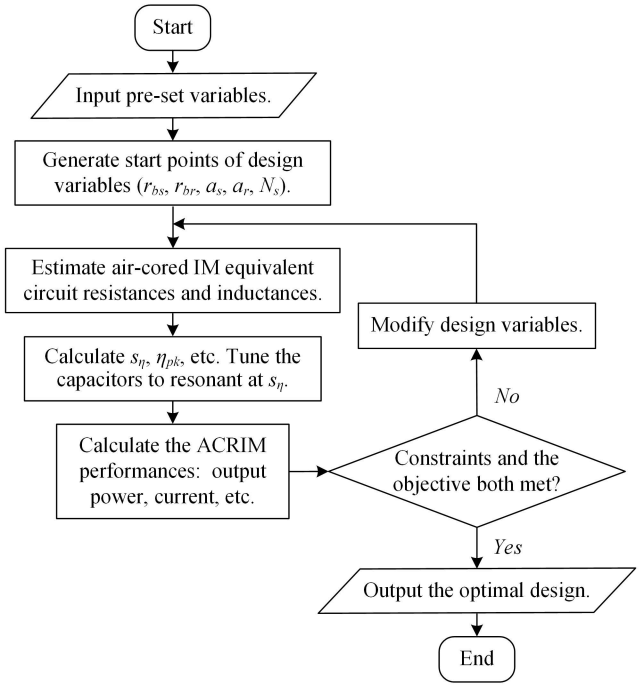

Fig. 4. Optimization procedure of an ACRIM.

IV. Optimization Results and Discussion

A. Baseline Design

In order to study the design trends and performance of ACRIMs under different tuning options, a number of optimized designs under different preset conditions are generated and compared. Firstly, setting the pole pair number of 3, aspect ratio of 1 and the conducting material of copper, the optimization is carried out with the objective to maximize the motoring-mode peak efficiency, the results are shown in TABLE III. Rounding errors can exist when values are recorded.

TABLE III. Baseline Design *

Parameter	Unit	Tuning I	Tuning II
r_{bs}	mm	52.50	52.50
r_{br}	mm	41.92	39.90
a_s	mm	12.07	10.60
a_r	mm	5.10	10.60
N_s	(Turns)	97	64
w	mm	94.42	92.40
R_s	mΩ	142.5	70.3
R_r	mΩ	383.0	82.0
L_s	μH	390.9	171.9
L_r	μH	397.7	152.7
M	μH	218.3	79.5
X_{ls}	Ω	2.169	1.160
X_m	Ω	2.743	0.999
X_{lr}'	Ω	2.254	0.920
C_s	μF	18.02	36.84
C_r	mF	/	8.364
η_{pk}	%	78.77	85.92
Vol.	dm^3	1.433	1.425
Mass	kg	5.272	5.871
η_{pk}/Mass	%/kg	14.94	14.64
P_m/Mass	kW/kg	1.897	1.703

* Objective: maximize η_{pk}; p_p = 3; k_{asp} = 1; n_s = 40k rpm; Copper wire.

L_s, L_r and M are the stator self-, rotor self- and magnetizing inductances in the equivalent circuit. C_s and C_r are the stator and rotor capacitance values. "Vol." is the estimation of volume of the air-cored IM, which is the sum of stator winding volume $V_{wdg,s}$, rotor winding volume, $V_{wdg,r}$, airgap volume, V_{ag} and the rotor inner volume $V_{r,in}$.

$$\begin{aligned} V_{wdg,s} &= 2\pi r_{bs} a_s w(1+k_{ew,s}) \\ V_{wdg,r} &= 2\pi r_{br} a_r w(1+k_{ew,r}) \\ V_{ag}+V_{r,in} &= \pi w((r_{bs}-a_s/2)^2 - 2a_r r_{br}) \end{aligned} \quad (21)$$

"Mass" is the active mass of the air-cored IM and is calculated as,

$$\text{Mass} = (h_{cond}k_f + h_{encap}(1-k_f))(V_{wdg,s}+V_{wdg,r}) \quad (22)$$

where h_{cond} is the density of conducting material, for copper, h_{cond} is 8960 kg/m^3, h_{encap} is the density of a lightweight epoxy encapsulation for support and is 900 kg/m^3. Both "Vol." and "Mass" include the end windings.

The designs in TABLE III are seen as the baseline for comparisons and are denoted as design I.0 and design II.0 in the following sections.

B. Extending Upper Bounds of Baseline Circle Radii

In TABLE III, the stator baseline circle radii r_{bs} in designs I.0 and II.0 reach the upper bound and they show the trend of expanding r_{bs} as much as possible, so more optimizations are carried out when the upper limit of r_{bs} is extended. As shown in TABLE IV, the upper bounds of r_{bs} and r_{br} in designs I.1 and II.1 are extended to 72.5 mm and 70.5 mm respectively, the upper bounds of r_{bs} and r_{br} in designs I.2 and II.2 are extended to 92.5 mm and 90.5 mm respectively.

TABLE IV. Comparison of Optimized Designs After Extending Upper Bounds of Baseline Circle Radii *

Parameter	Tuning I			Tuning II		
	I.0	I.1	I.2	II.0	II.1	II.2
r_{bs} (mm)	52.50	72.50	92.50	52.50	72.50	92.50
r_{br} (mm)	41.92	58.61	75.29	39.90	55.74	71.58
a_s (mm)	12.07	16.80	21.51	10.60	14.76	18.92
a_r (mm)	5.10	6.98	8.90	10.60	14.76	18.92
N_s (turns)	97	88	79	64	56	50
w (mm)	94.42	131.11	167.79	92.40	128.24	164.08
R_s (mΩ)	142.5	84.0	53.5	70.3	37.8	23.3
R_r (mΩ)	383.0	228.0	145.1	82.0	43.9	26.9
L_s (μH)	390.9	443.1	461.0	171.9	177.9	179.0
L_r (μH)	397.7	454.1	474.1	152.7	158.9	160.3
M (μH)	218.3	258.7	275.8	79.5	85.7	88.3

TABLE IV (continued).

X_{ls} (Ω)	2.169	2.317	2.328	1.160	1.158	1.141
X_m (Ω)	2.743	3.250	3.465	0.999	1.077	1.109
X_{lr}' (Ω)	2.254	2.456	2.492	0.920	0.919	0.905
C_s (μF)	18.02	16.08	15.55	36.84	35.59	35.37
C_r (mF)	/	/	/	8.364	30.058	81.173
η_{pk} (%)	78.77	88.64	93.04	85.92	92.72	95.59
Vol. (dm^3)	1.433	3.804	7.935	1.425	3.789	7.914
Mass (kg)	5.272	14.043	29.365	5.871	15.738	33.015
η_{pk}(%)/kg	14.94	6.31	3.17	14.64	5.89	2.90
kW/kg	1.897	0.712	0.341	1.703	0.635	0.303

* Objective: maximize η_{pk}; $p_p = 3$; $k_{asp} = 1$; $n_s = 40$k rpm; Copper wire; Upper bound of r_{bs} and r_{br} in designs I.1 and II.1 are extended to 72.5 mm and 70.5 mm respectively, the upper bound of r_{bs} and r_{br} in designs I.2 and II.2 are extended to 92.5 mm and 90.5 mm respectively.

It can be seen that the optimization results always push the r_{bs} values to their upper bound. This is because when the objective is to maximize η_{pk}, the optimization procedure tends to put as much copper into the stator that meets the constraints: Air-cored IMs have a low value of magnetizing reactance and this means the stator draws a large magnetizing current. In a well-designed iron-cored IM, the magnetizing reactance is high and the magnetizing current is low, the input stator current is then dominated by the load current which develops the torque. For the air-cored IM designs, the stator current is dominated by the large magnetizing current. The design optimization therefore seeks to minimize the stator resistance to reduce the losses caused by the high magnetizing current by putting more copper into the stator, as a result, pushing r_{bs} to its upper bound. Increasing a_s also reduces stator resistance, but larger a_s pulls the stator and rotor baseline circles apart which consequently reduces the stator-to-rotor mutual coupling and in turn, reduces the efficiency.

C. Modifying the Objective

As shown in TABLE IV, when the objective is to maximize η_{pk}, r_{bs} becomes more like a manually-set parameter rather than a degree of freedom because the design always reaches the upper bound of r_{bs}. A smaller r_{bs} results in a more compact design with a higher power-to-weight ratio kW/kg but lower η_{pk}. In order to force the optimization procedure to balance the efficiency and active mass, in TABLE V, the objectives are modified to maximize the peak efficiency per unit mass, η_{pk}/Mass, for designs I.3 and II.3, and η_{pk}/Mass with the efficiency constraint for designs I.4 and II.4.

TABLE V. COMPARISON OF OPTIMIZED DESIGNS AFTER CHANGING THE OPTIMIZATION OBJECTIVE *

Parameter	Tuning I			Tuning II		
	I.0	I.3	I.4	II.0	II.3	II.4
r_{bs} (mm)	52.50	23.79	52.50	52.50	23.28	49.23
r_{br} (mm)	41.92	20.65	47.46	39.90	19.90	43.89
a_s (mm)	12.07	1.28	3.93	10.60	1.25	3.14
a_r (mm)	5.10	1.02	2.15	10.60	1.49	3.54
N_s (turns)	97	30	60	64	32	44
w (mm)	94.42	44.44	99.96	92.40	43.18	93.11
R_s (mΩ)	142.5	131.0	174.0	70.3	150.4	111.9
R_r (mΩ)	383.0	177.6	336.9	82.0	137.9	105.9
L_s (μH)	390.9	20.8	181.1	171.9	23.0	89.1
L_r (μH)	397.7	20.1	186.0	152.7	21.0	83.5
M (μH)	218.3	13.0	138.3	79.5	13.6	63.0
X_{ls} (Ω)	2.169	0.0984	0.539	1.160	0.118	0.328
X_m (Ω)	2.743	0.163	1.737	0.999	0.171	0.791
X_{lr}' (Ω)	2.254	0.0893	0.600	0.920	0.0935	0.259
C_s (μF)	18.02	327.54	41.66	36.84	275.67	71.11
C_r (mF)	/	/	/	8.364	1.960	5.265
η_{pk} (%)	78.77	15.88	70.00	85.92	21.61	76.00
Vol. (dm^3)	1.433	0.0948	1.086	1.425	0.0901	0.897
Mass (kg)	5.272	0.148	1.995	5.871	0.164	1.858
η_{pk}(%)/kg	14.94	107.42	35.08	14.64	132.06	40.90
kW/kg	1.897	67.629	5.011	1.703	61.125	5.382

* Objective of designs I.3 and II.3 is to maximize η_{pk}/Mass, objective of designs I.4 and II.4 is to maximize η_{pk}/Mass under the efficiency constraint of higher than 70% and 76% respectively; $p_p = 3$; $k_{asp} = 1$; $n_s = 40$k rpm; Copper wire.

When the objective is to maximize η_{pk}/Mass, as shown in designs I.3 and II.3, the optimization procedure generates light-weight designs with very high η_{pk}/Mass values but very low efficiencies of around 20%. So a minimum η_{pk} value constraint was added: minimum η_{pk} values were set at 70% and 76% for tuning options I and II respectively, these values are selected based on the original designs of I.0 and II.0. It can be seen that the kW/kg values are improved at the expense of peak efficiency.

D. Modifying the Number of Pole Pairs

As shown in TABLE VI, considering the number of slots is 36 for both stator and rotor, only two other pole pair numbers are chosen here, namely one pole-pair for designs I.5 and II.5, and six pole-pairs for designs I.6 and II.6.

TABLE VI. COMPARISON OF OPTIMIZED DESIGNS AFTER CHANGING THE NUMBER OF POLE PAIRS *

Parameter	Tuning I			Tuning II		
	I.5	I.0	I.6	II.5	II.0	II.6
r_{bs} (mm)	52.50	52.50	52.50	52.50	52.50	52.50
r_{br} (mm)	33.41	41.92	45.35	31.69	39.90	44.06
a_s (mm)	23.80	12.07	6.90	18.81	10.60	6.44
a_r (mm)	10.38	5.10	3.40	18.81	10.60	6.44
N_s (turns)	75	97	96	48	64	69
w (mm)	85.91	94.42	97.85	84.19	92.40	96.56
R_s (mΩ)	61.6	142.5	194.6	31.9	70.3	104.8
R_r (mΩ)	168.8	383.0	438.0	39.0	82.0	118.7
L_s (μH)	1296.2	390.9	138.6	535.4	171.9	70.9
L_r (μH)	1024.6	397.7	160.4	398.7	152.7	66.4
M (μH)	705.5	218.3	84.9	267.5	79.5	35.3
X_{ls} (Ω)	2.474	2.169	1.349	1.122	1.160	0.894
X_m (Ω)	2.955	2.743	2.134	1.120	0.999	0.888
X_{lr}' (Ω)	1.336	2.254	1.896	0.550	0.920	0.782
C_s (μF)	49.38	18.02	12.85	106.45	36.84	22.33
C_r (mF)	/	/	/	153.27	8.364	1.941
η_{pk} (%)	91.39	78.77	67.61	93.89	85.92	77.84
Vol. (dm^3)	2.643	1.433	1.095	2.410	1.425	1.096

TABLE VI (continued).

Mass (kg)	13.681	5.272	2.585	12.814	5.871	3.052
η_{pk}(%)/kg	6.68	14.94	26.16	7.33	14.64	25.51
kW/kg	0.731	1.897	3.869	0.780	1.703	3.277

* Objective: maximize η_{pk}; $p_p = 1$ for designs I.5 and II.5, $p_p = 6$ for designs I.6 and II.6; $k_{asp} = 1$; $n_s = 40$k rpm; Copper wire.

It can be seen that, when the number of pole pairs increases, the power-to-weight ratio, kW/kg value, increases, but the η_{pk} value and magnetizing reactance decreases though higher pole numbers results in a higher supply frequency. Also, all L_s, L_r and M values decrease. According to [13], the magnetic flux density produced by an air-cored cylindrical current sheet decays by a factor of $(r/r_0)^{pp-1}$ in the region inside the winding and by a factor of $(r_0/r)^{pp+1}$ in the region outside the winding, where r_0 is the winding radius and r is the field point radius [13]. When the number of pole pairs p_p increases, the magnetic flux density falls off more rapidly, so the stator-to-rotor magnetic coupling becomes weaker and the efficiency suffers.

E. Modifying the Synchronous Speed

TABLE VII shows optimized designs with different synchronous speed, for designs I.7 and II.7, the synchronous speed is 30k rpm, for designs I.8 and II.8, the synchronous speed is 50k rpm.

TABLE VII. COMPARISON OF OPTIMIZED DESIGNS AFTER CHANGING THE SYNCHRONOUS SPEED *

Parameter	Tuning I			Tuning II		
	I.7	I.0	I.8	II.7	II.0	II.8
r_{bs} (mm)	52.50	52.50	52.50	52.50	52.50	52.50
r_{br} (mm)	41.88	41.92	41.94	39.90	39.90	39.90
a_s (mm)	12.04	12.07	12.08	10.60	10.60	10.60
a_r (mm)	5.20	5.10	5.03	10.60	10.60	10.60
N_s (turns)	105	97	90	72	64	59
w (mm)	94.38	94.42	94.44	92.40	92.40	92.40
R_s (mΩ)	168.6	142.5	122.8	88.9	70.3	58.0
R_r (mΩ)	442.9	383.0	334.7	103.7	82.0	67.7
L_s (μH)	461.6	390.9	337.2	217.4	171.9	141.9
L_r (μH)	468.0	397.7	343.8	193.2	152.7	126.1
M (μH)	256.8	218.3	188.7	100.6	79.5	65.7
X_{ls} (Ω)	1.930	2.169	2.332	1.101	1.160	1.197
X_m (Ω)	2.420	2.743	2.965	0.948	0.999	1.031
X_{lr}' (Ω)	1.991	2.254	2.435	0.872	0.920	0.949
C_s (μF)	27.07	18.02	13.39	51.78	36.84	28.57
C_r (mF)	/	/	/	6.955	8.364	9.830
η_{pk} (%)	73.19	78.77	82.43	81.69	85.92	88.56
Vol. (dm^3)	1.433	1.433	1.433	1.425	1.425	1.425
Mass (kg)	5.287	5.272	5.264	5.871	5.871	5.871
η_{pk}(%)/kg	13.84	14.94	15.66	13.92	14.64	15.09
kW/kg	1.892	1.897	1.900	1.703	1.703	1.703

* Objective: maximize η_{pk}; $p_p = 3$; $k_{asp} = 1$; Copper wire; $n_s = 30$k rpm for designs I.7 and II.7, $n_s = 50$k rpm for designs I.8 and II.8.

It can be seen from TABLE VII that, changing the synchronous speed enhances the η_{pk} value but does not significantly vary kW/kg value and the electromagnetic design, the total volume and active mass almost stay the same. For the different designs under the tuning option I, it is more like re-winding an air-cored IM with different number of turns. However, it is worth mentioning that, for mechanical reasons, the airgap length may have to be increased when the rotor needs to operate at higher speed, then reducing the mutual coupling between the stator and rotor windings.

F. Changing the Aspect Ratio

Optimizations are also carried out when different aspect ratios are set, for designs I.9 and II.9, $k_{asp} = 0.3$, for designs I.10 and II.10, $k_{asp} = 3$. The results are compared in TABLE VIII.

TABLE VIII. COMPARISON OF OPTIMIZED DESIGNS AFTER CHANGING THE ASPECT RATIO *

Parameter	Tuning I			Tuning II		
	I.9	I.0	I.10	II.9	II.0	II.10
r_{bs} (mm)	52.50	52.50	52.50	52.50	52.50	52.50
r_{br} (mm)	41.48	41.92	42.58	39.52	39.90	40.56
a_s (mm)	12.67	12.07	11.11	10.98	10.60	9.94
a_r (mm)	5.36	5.10	4.73	10.98	10.60	9.94
N_s (turns)	61	97	127	40	64	86
w (mm)	313.27	94.42	31.69	306.72	92.40	31.02
R_s (mΩ)	121.2	142.5	171.6	59.3	70.3	87.3
R_r (mΩ)	346.7	383.0	429.6	74.6	82.0	94.3
L_s (μH)	400.9	390.9	370.8	172.5	171.9	171.3
L_r (μH)	419.9	397.7	364.4	161.5	152.7	142.5
M (μH)	234.3	218.3	194.6	85.0	79.5	73.0
X_{ls} (Ω)	2.094	2.169	2.214	1.100	1.160	1.235
X_m (Ω)	2.944	2.743	2.446	1.068	0.999	0.917
X_{lr}' (Ω)	2.333	2.254	2.134	0.962	0.920	0.874
C_s (μF)	17.67	18.02	18.85	36.70	36.84	36.98
C_r (mF)	/	/	/	11.447	8.364	5.528
η_{pk} (%)	82.45	78.77	73.01	88.30	85.92	82.07
Vol. (dm^3)	3.843	1.433	0.723	3.709	1.425	0.754
Mass (kg)	12.525	5.272	3.116	13.858	5.871	3.512
η_{pk}(%)/kg	6.58	14.94	23.43	6.37	14.64	23.37
kW/kg	0.798	1.897	3.209	0.722	1.703	2.848

* Objective: maximize η_{pk}; $p_p = 3$; $k_{asp} = 1$; $n_s = 40$k rpm; Copper wire; $k_{asp} = 0.3$ for designs I.9 and II.9, $k_{asp} = 3$ for designs I.10 and II.10.

As shown in TABLE VIII, higher aspect ratio results in lower η_{pk} value but higher power-to-weight ratio, because higher aspect ratio reduces the machine axial length thus reduces the total active mass value. The impact of the end windings is also greater when the aspect ratio is higher.

G. Changing the Conducting Material

The designs I.11 and II.11 in TABLE IX shows the optimization results when the conducting material changes to aluminum which has a higher resistivity but a lower density than copper.

It can be seen that, changing conducting material does not significantly vary the optimization results of the electromagnetic design variables, except for the number of turns. ACRIMs which use aluminum wires have higher stator

and rotor resistances and lower η_{pk} value compared to copper-wire designs, but they almost triple the power-to-weight ratio of the air-cored IM because of the reduction in active mass.

TABLE IX. COMPARISON OF OPTIMIZED DESIGNS AFTER CHANGING TO THE ALUMINUM WIRE *

Parameter	Tuning I		Tuning II	
	I.0	I.11	II.0	II.11
r_{bs} (mm)	52.50	52.50	52.50	52.50
r_{br} (mm)	41.92	41.85	39.90	39.90
a_s (mm)	12.07	12.02	10.60	10.60
a_r (mm)	5.10	5.27	10.60	10.60
N_s (turns)	97	88	64	62
w (mm)	94.42	94.35	92.40	92.40
R_s (mΩ)	142.5	181.3	70.3	99.4
R_r (mΩ)	383.0	469.7	82.0	116.0
L_s (μH)	390.9	321.8	171.9	157.8
L_r (μH)	397.7	325.6	152.7	140.2
M (μH)	218.3	178.6	79.5	73.0
X_{ls} (Ω)	2.169	1.799	1.160	1.065
X_m (Ω)	2.743	2.244	0.999	0.917
X_{lr}' (Ω)	2.254	1.847	0.920	0.844
C_s (μF)	18.02	21.81	36.84	40.14
C_r (mF)	/	/	8.364	4.166
η_{pk} (%)	78.77	70.02	85.92	79.17
Vol. (dm^3)	1.433	1.433	1.425	1.425
Mass (kg)	5.272	1.828	5.871	2.026
η_{pk}(%)/kg	14.94	38.31	14.64	39.07
kW/kg	1.897	5.471	1.703	4.935

* Objective: maximize η_{pk}; p_p = 3; k_{asp} = 1; n_s = 40k rpm; Designs I.11 and II.11 use aluminum wire.

V. CONCLUSION

This paper proposes a design optimization procedure based on a computationally-fast, 3D-FEA-free inductance calculation method using closed-form solutions of Neumann integrals. The equivalent circuit parameters are estimated using the idealized coil shapes. The optimizations are carried out for two different capacitor tuning options. The time required to generate one optimized design on a PC with an i7 CPU (3.4 GHz) and 16 GB RAM is usually less than 20 min, which is much faster than a complete optimization based on 3-D FEA. The comparison of the design results using the two tuning options with different pre-set parameters shows that, under the same condition, tuning option II has higher peak efficiency values than tuning option I, but option II has very large rotor capacitors of several millifarad. If the whole ACRIM including the capacitors is regarded as a system, option II does not have significant advantage in the system power density (kW/kg) than tuning option I which uses stator capacitors only. Tuning option I is also more practical as it avoids connecting or mounting capacitors to a high-speed rotor.

REFERENCES

[1] Y. Fujimoto, "Modeling and analysis of wireless electro-mechanical energy transfer and conversion using resonant inductive coupling," *IECON 2015 - 41st Annual Conference of the IEEE Industrial Electronics Society*, Yokohama, 2015, pp. 4905-4910.

[2] B. J. Ebot and Y. Fujimoto, "A General Framework for the Analysis and Design of a Wireless Resonant Motor," *2019 IEEE International Electric Machines & Drives Conference (IEMDC)*, San Diego, CA, USA, 2019, pp. 1966-1970.

[3] K. Takishima and K. Sakai, "Equivalent Circuit Analysis of an Ultra-Lightweight Motor Designed with Magnetic Resonance Coupling," *2018 20th European Conference on Power Electronics and Applications (EPE'18 ECCE Europe)*, Riga, 2018, pp. P.1-P.9.

[4] K. Sakai, T. Akiyama and K. Takijima, "Basic Characteristics of an Ultra-lightweight Magnetic Resonance Coupling Machine with a Cage Rotor," *2018 International Symposium on Power Electronics, Electrical Drives, Automation and Motion (SPEEDAM)*, Amalfi, 2018, pp. 268-273.

[5] K. Takishima and K. Sakai, "Starting characteristics of axial and radial type ultra-lightweight motors based on magnetic resonance coupling," in *IEEJ Journal of Industry Applications*, vol. 8, no. 3, pp. 471-479, 2019.

[6] K. Takishima and K. Sakai, "Analytical and Experimental Investigation of the Frequency Characteristics of an Ultra-Lightweight Motor Based on Magnetic-Resonance Coupling," *2018 XIII International Conference on Electrical Machines (ICEM)*, Alexandroupoli, 2018, pp. 562-568.

[7] M. Liu, K. W. Chan, J. Hu, Q. Lin, J. Liu and W. Xu, "Design and Realization of a Coreless and Magnetless Electric Motor Using Magnetic Resonant Coupling Technology," in *IEEE Transactions on Energy Conversion*, vol. 34, no. 3, pp. 1200-1212, Sept. 2019.

[8] M. F. Iacchetti, R. P. Deodhar, A. C. Smith and K. Mishima, "Modelling and Operating Characteristics of Air-Cored Resonant Induction Machines," *2018 IEEE Energy Conversion Congress and Exposition (ECCE)*, Portland, OR, 2018, pp. 6468-6475.

[9] Z. Jin, M. F. Iacchetti, A. C. Smith, R. P. Deodhar and K. Mishima, "Comparison of Different Capacitor Tuning Criteria in Air-Cored Resonant Induction Machines," *2019 IEEE Energy Conversion Congress and Exposition (ECCE)*, Baltimore, MD, USA, 2019, pp. 3017-3024.

[10] Z. Jin, M. F. Iacchetti, A. C. Smith, R. P. Deodhar, Y. Komi, A. A. Abduallah, C. Umemura, K. Mishima, "Air-Cored Resonant Induction Machines: Comparison of Capacitor Tuning Criteria and Experimental Validation," in *IEEE Transactions on Industry Applications*, Early Access 2021, doi: 10.1109/TIA.2021.3075646.

[11] Z. Jin, M. F. Iacchetti, A. C. Smith, R. P. Deodhar, Y. Komi, A. A. Abduallah, C. Umemura, "Winding Inductance Estimations in Air-Cored Resonant Induction Machines," *2020 IEEE Energy Conversion Congress and Exposition (ECCE)*, Detroit, MI, USA, 2020, pp. 5813-5820.

[12] F. W. Grover, *Inductance calculations: working formulas and tables*. Courier Corporation, 2004.

[13] A. Hughes and T. J. E. Miller, "Analysis of fields and inductances in air-cored and iron-cored synchronous machines," in *Proceedings of the Institution of Electrical Engineers*, vol. 124, no. 2, pp. 121-126, Feb. 1977.